

Competition between inter and intramolecular hydrogen bond evidenced by vibrational circular dichroism spectroscopy: The case of (1S,2R)-(−)-cis-1-amino-2-indanol

Katia Le Barbu-Debus, Anne Zehnacker

▶ **To cite this version:**

Katia Le Barbu-Debus, Anne Zehnacker. Competition between inter and intramolecular hydrogen bond evidenced by vibrational circular dichroism spectroscopy: The case of (1S,2R)-(−)-cis-1-amino-2-indanol. Chirality, 2021, 10.1002/chir.23362 . hal-03356734

HAL Id: hal-03356734

https://universite-paris-saclay.hal.science/hal-03356734

Submitted on 28 Sep 2021

HAL is a multi-disciplinary open access archive for the deposit and dissemination of scientific research documents, whether they are published or not. The documents may come from teaching and research institutions in France or abroad, or from public or private research centers.

L'archive ouverte pluridisciplinaire **HAL**, est destinée au dépôt et à la diffusion de documents scientifiques de niveau recherche, publiés ou non, émanant des établissements d'enseignement et de recherche français ou étrangers, des laboratoires publics ou privés.

Competition between Inter and Intramolecular Hydrogen Bond Evidenced by Vibrational Circular Dichroism Spectroscopy. The Case of *(1S,2R)*-(-)-*cis*-1-amino-2-indanol

Abstract: The infra-red (IR) absorption and vibrational circular dichroism (VCD) spectra of an intramolecularly hydrogen-bonded chiral amino-alcohol, (1*S*,2*R*)-(-)-*cis*-1-amino-2-indanol, are studied in DMSO-d_6. The spectra are simulated at the DFT level within the frame of the cluster-in-the-liquid model. Both IR and VCD spectra show a clear signature of the formation of intermolecular hydrogen bonds at the detriment of the intramolecular OH…N interaction present in the isolated molecule. Two solvent molecules are necessary to reproduce the experimental spectra. While the first DMSO molecule captures the main spectral modifications due to hydrogen bond formation between the solute and the solvent, the second DMSO molecule is necessary for a good description of the Boltzmann contribution of the different complexes, based on their Gibbs free energy.

Katia Le Barbu-Debus,[a] and Anne Zehnacker *[a]

Keywords: Hydrogen bond- IR spectroscopy - Molecular interactions - Solvation - Chiroptical Spectroscopy.

Introduction

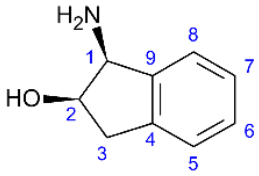
Intramolecular hydrogen bond (H-bond) formation is of prime importance for shaping the structure of biomolecules and biopolymers such as proteins.[1,2] Depending on the nature of the donor and the acceptor and the geometrical constraints between them, the intramolecular interactions, among which NH…O, OH….O, and OH…N bridges, range from strong H-bonds to weaker contacts that hardly influence the IR frequencies.[3,4] Interaction with a H-bond donor or acceptor environment results in a competition between intra and intermolecular H-bond formation. The intramolecular H-bond may be disrupted to the benefit of intermolecular H-bond formation, or not, depending on the relative interaction energies and experimental conditions. The competition between intra- and inter-molecular H-bond formation has been the subject of numerous studies in weakly bound complexes isolated in the gas phase, under supersonic jet conditions.[5-7] The 1-2 amino-alcohol motif is in particular an interesting prototype for these studies, due to its ubiquity in biomolecules such as neurotransmitters. Different structures are observed for the jet-cooled complexes of 1-2 aminoalcohols with H-bond donating or accepting molecules.[8-14] In the so-called addition complex, the solvent interacts with the internally bound aminoalcohol without modifying its structure, while in the insertion complexes, the intramolecular H-bond opens up so that both hydroxyl and amino groups interact with the solvent in a bidentate manner.[15] Both structures are observed under jet-cooled conditions because the energy barrier required for opening the H-bond may be insurmountable at the low temperature achieved there. In contrast, intermolecular interactions dominate in the bulk.[16]

Vibrational circular dichroism (VCD), *i.e.* the difference in IR absorption by a chiral molecule between left and right circular polarized light, is a very sensitive probe of conformational flexibility and molecular interactions. H-bonding in particular strongly impinges the shape of VCD spectra.[17] The influence of H-bond formation is observed in the solid state where strong intermolecular interactions take place[18-21] and also in matrix isolation spectroscopy[22-26] or in solution studies.[27-29] The VCD spectrum of rigid systems in solution can be reproduced by the contribution of a limited number of structures. The same approach holds to some extent for solid-state systems where a small aggregate in the geometry of the crystal accounts qualitatively well for the measured spectrum,[21,30] although this approach does not include long-range couplings.[31] Temperature and anharmonicity effects influence the shape of the VCD spectra of flexible systems in solution. This aspect is especially important for simulating the VCD spectrum of hydroxyl-containing molecules, whose OH bend region is very sensitive to structural dynamics.[32] Molecular dynamics approaches have been proposed to account for these effects, which rest either on force fields or on first-principle simulations.[33-37] However, they are often computationally demanding, in particular for complex or large molecules. An efficient alternative has been proposed, which consists in approximating the solute/solvent system by a limited number of clusters of well-defined size and shape, embedded in a solvent continuum. This approach is especially relevant for protic molecules diluted in a polar solvent, where specific and strong H-bonding interactions dictate the geometry of the clusters. This model, referred to as the "cluster-in-the-liquid" model in the literature, has been successfully introduced for small molecules like glycidol or methyl lactate in water,[38,39]

[a] *Dr. Katia Le Barbu-Debus, Dr; A. Zehnacker*
Institut des Sciences Moléculaires d'Orsay
Université Paris-Saclay, CNRS.
91405, Orsay, France
E-mail: anne.zehnacker-rentien@universite-paris-saclay.fr

Received: ((will be filled in by the editorial staff))
Revised: ((will be filled in by the editorial staff))
Published online: ((will be filled in by the editorial staff))

then further applied to many systems, including large molecules.[40,41] Recent simulations based on first-principles molecular dynamics have confirmed the existence of long-lived 1:1 complexes, which gives further validation to the "cluster-in-the-liquid" model.[37] We apply here this approach to (1*S*,2*R*)-(-)-*cis* 1-amino-2-indanol (*cis*-AI), a bifunctional indane derivative endowed with an intramolecular H-bond shown in Scheme 1. This molecule has two stereogenic centers located on each functional carbons, which are of opposite absolute configuration. The structure of *cis* 1-amino-2-indanol as well as its hydrate is well known in the gas phase.[10,13,42,43] Due to the conformational bias introduced by the alicyclic ring, the OH and NH_2 substituents can only be in axial/equatorial or equatorial/axial positions. Two almost isoenergetic monomers have been observed under supersonic jet conditions, both showing a frustrated intramolecular H-bond. They are related by the indane ring puckering (see Figure 1). Formation of *cis*-AI hydrates under jet-cooled conditions occurs through addition of the water molecule, keeping the intramolecular H-bond intact,[13] while complexation with methyl-lactate takes place through both insertion or addition processes.[10] No VCD spectra have been reported so far for *cis*-AI, although those of the related molecules 1-indanol, 1-methylindane, 1-aminoindane and *trans* 1-amino-2-indanol (*trans*-AI) are known from previous work.[37,44-46] Polavarapu and co-workers have paid particular attention to the role of the puckering motion and the rotation of the amino group in shaping the VCD spectra of neat 1-aminoindane, which was well reproduced by the Boltzmann weighted average contributions of the six most stable monomers.[44] The IR absorption and VCD spectra of 1-indanol in DMSO have been simulated by both first-principle molecular dynamics simulations and the cluster-in-the-liquid approach.[37,44] The VCD spectrum was well reproduced by the Boltzmann-averaged contributions of the most stable 1:1 complexes resulting from a full exploration of the potential energy surface, embedded in a DMSO solvent continuum. All the calculated 1:1 complexes, in both the Le Barbu-Debus *et al.* and Johnson *et al.* works, involve a strong OH…O H-bond from the 1-indanol hydroxyl to the DMSO.[37,44] Taking into account larger clusters was not necessary to reproduce the VCD spectrum. The case of bifunctional compounds like diols or amino-alcohols might be different because they possess two protic substituents that could interact with the solvent. It has been shown for chiral diols that, depending on the strength of the intramolecular H-bond, one to two solvent molecules should be explicitly included for accounting for the experimental spectra.[47] Explicit solvation was not even necessary to determine the absolute configuration of a cyclic diol in methanol, which was treated as a continuum.[48] We have recently discussed the influence of solvation on the IR absorption and VCD spectrum of (1*S,2S*)-*trans*-1-amino-2-indanol (*trans*-AI), a stereomer of *cis*-AI. Static calculations resting on the cluster-in-the-liquid model were assessed by comparison with first principles and force fields molecular dynamics descriptions of solvation.[46] The main conclusions of this work was that the VCD signal was mainly local, with no contribution of the solvent to the electric and magnetic dipole moments. The 1:1 complexes were able to capture the main features of solvation and satisfactorily reproduce the VCD spectrum, provided that their contributions to the VCD spectrum are correct. In other words, the VCD spectrum of each conformer was not strongly modified by solvation but its contribution to the total VCD spectrum, dictated by the Boltzmann factors, *i.e.*, the relative Gibbs energy, was modified by solvation. In this work, we apply the cluster-in-the-liquid model to *cis*-AI in DMSO. *cis*-AI differs from *trans*-AI by the presence of an intramolecular H-bond which is absent in *trans*-AI. This raises the question of the competition between inter and intramolecular H-bond. Based on cluster-in-the-liquid calculations, we will discuss the following points: what is the size of the clusters that should be taken into consideration to satisfactorily reproduce the spectra? What are the intramolecular and intermolecular factors influencing the shape of the VCD spectra in this system, such as the puckering angle, the orientation of the substituents? Last, can VCD spectroscopy be used as a signature of the H-bond formation with the solvent, to the detriment of the intramolecular interaction observed in the gas phase? To this end, we will compare the experimental IR absorption and VCD spectra of *cis*-AI in DMSO to those simulated for the monomer and clusters of different size, resorting to density functional theory (DFT) methods including, or not, dispersion corrections.



SCHEME 1 Structure of *cis*-AI and atom numbering.

Materials and Methods

Experimental: The vibrational IR absorption and VCD spectra were measured with a Fourier Transform Infra-Red (FTIR) spectrometer Vertex 70 (Bruker) equipped with a VCD module PMA 50 (Bruker). The signal was measured by a MCT IR detector with a BaF_2 window, cooled with liquid nitrogen. A spectral resolution of 4 cm^{-1} was used for both absorption and VCD spectra. The IR radiation was polarized with a linear polarizer then modulated by a 50 kHz ZnSe photo-elastic modulator (Hinds). Insertion of a 2000 cm^{-1} low-pass filter before the linear polarizer resulted in an increase of the dynamical response of the detector. The signal of the MCT detector was demodulated using a lock-in amplifier (Stanford Research Systems SR 830). The spectra were measured using 1 M solutions in DMSO-d6 in a 56 μm cell with an acquisition time of 4 h. The used concentration corresponds to the saturation limit at room temperature and to an optical density of ~0.4 for the larger-intensity band at 1475 cm^{-1}. The alignment of the spectrometer was controlled by checking the mirror-image relation between the VCD spectra of the two enantiomers of camphor (0.3 M in CCl_4) in the same cell as used here. DMSO-d6 and enantiopure (1*R*,2*S*)-(+)-*cis*-1-amino-2-indanol (1*S*,2*R*)-(-)-*cis*-1-amino-2-indanol (99% purity) were purchased by Aldrich and used without further purification.

Theoretical: The exploration of the potential energy surface of the clusters was performed using the Macromodel program and the graphical interface Maestro of the Schrödinger package.[49,50] For each system, monomer or complex, several explorations were performed using the advanced conformation search option, with either the MMffs or the OPLS2005 force fields.[51,52] Then the "redundant isomer" option was used to reduce the number of isomers. The root-mean-square deviation used was 1.0 Å for the *cis*-AI/DMSO complex and 1.5 Å for the *cis*-AI/$DMSO_2$ complex. All the isomers below 5 kcal mol^{-1} obtained thereby for the 1:1 or 1:2 complexes were then fully optimized in the frame of the DFT including empirical dispersion (DFT-D3BJ) or not.[53,54] Both

B3LYP/6-311++G(d,p) and B3LYP-D3BJ/6-311++G(d,p) levels.[55-57] were used to assess the influence of dispersion corrections on the calculated structures and spectra. Additional structures, which do not contribute through their Boltzmann population, were also optimized for the monomer and the 1:1 complex: For the sake of comparison between complexes of different sizes containing the same monomer conformation, we fully optimized 1:1 complexes resulting from 1:2 complex from which we remove one DMSO, and monomers resulting from a 1:1 complex from which we remove a DMSO. All structures were calculated in a DMSO solvent continuum with the Polarizable Continuum Model (PCM) default option of Gaussian.[58] The harmonic frequencies were calculated at the same level of theory for structures corresponding to true minima, and scaled by 0.98 to account for anharmonicity and basis set incompleteness. The energetic values given in the text are the Gibbs energy at 298.15 K (ΔG) when not specified otherwise. Zero-point-energy (ZPE) corrected energies (ΔE_0) have also been considered. All the calculations were performed with the Gaussian 09, Revision D.01 software.[59] The monomers and complexes described below are those with relative Gibbs energy below 1.5 kcal mol^{-1}, unless specified otherwise.

Results and Discussion

RESULTS

Molecular Structure and Solvation Network

Nomenclature

In what follows, we resort to the nomenclature already used for (1*R*,2*R*)-(-)-*trans*-1-amino-2-indanol.[46] It is based first on the orientation of the five-member ring. The configuration is called **eq**, for equatorial, when the amino group is in equatorial position, the hydroxyl group being in axial position. Conversely, the geometry is called **ax**, for axial, when the amino group is in axial position and the hydroxyl group in equatorial. The orientation of the hydroxyl group is denoted by g^+, g^- or t depending on the value of the HC_2OH dihedral angle (around 60°, -60° and 180°, respectively). Similarly, the amino group orientation is denoted by G^+, G^- and T when the HC_1Nlp dihedral angle is around 60°, -60° and 180°, respectively; lp standing for the lone pair of the nitrogen atom. Two additional notations are introduced here, t* and T*. They correspond to a geometry with the C_1C_2OH and the C_2C_1Nlp dihedral angles close to 0°, respectively.

In what follows, the 1:1 complexes are denoted bi-monomer, $mono_{OH}$-monomer or $mono_{NH}$-monomer and noHB-monomer. The suffix monomer describes the structure of the monomer contained in the complex. The prefix $mono_{OH}$, $mono_{NH}$, and noHB describes the presence of an intermolecular H-bond with OH, NH, or no intermolecular H bond, respectively. The prefix bi means that both OH and NH groups are bonded to the same DMSO molecule. The 1:2 complexes are called in the same manner, *i.e.* $mono_{OH}$-$mono_{NH}$-monomer when both DMSO molecule are H-bonded to *cis*-AI, and simply dmso added to the name of the 1:1 complex when the second DMSO molecule is not directly bonded to *cis*-AI. When none of the DMSO molecules is directly bonded to *cis*-AI, the geometry is denoted noHB-monomer. Each structure, characterized by a given molecular geometry and an H-bond pattern, displays variants, related to the internal rotation of the solvent. We call this ensemble a "family". We have noticed that the IR absorption and VCD spectra are identical for a given family. Therefore, we shall only describe and discuss one geometry per family, which is defined by its H-bond pattern and a given intramolecular geometry. However, we calculate the Boltzmann weights using the total population, including all the variants found for a family, due to the flexibility associated with the solvation pattern. In what follows the term "family" will be omitted for the sake of simplicity.

Monomer

In the gas phase, the two most stable calculated structures display an OH…N intramolecular H-bond and differ by the ring puckering geometry. The most stable conformer has NH_2 in axial and OH in equatorial positions. It is called **ax**t*G^+ and is identical to the *cis*-AI_I conformer previously reported.[43] The second one has NH_2 in equatorial and the OH in axial and the position is called **eq**g^-T* and is the *cis*-AI_{II} previously reported.[43] The energy gap between theses conformers is of the order of 0.5 kcal mol^{-1}, which is compatible with their coexistence under supersonic jet conditions.[42,43] Only these two conformers are obtained below 2 kcal mol^{-1}.

Inclusion of a DMSO solvent continuum inverts the energy ordering between these conformers relative to the gas phase but the energy difference is still small, **eq**g^-T* being more stable than **ax**t*G^+ by ~ 0.3 kcal mol^{-1}. The relative Gibbs energies of the different conformers is similar when including dispersion corrections or not and are summarized in Table 1. Considering the relative zero-point-energy (ZPE) corrected energies does not modify the energetic preference. Solvation also stabilizes additional forms of the *cis*-AI monomer, shown in Figure 1. Although they are higher in energy by more than 1.5 kcal mol^{-1}, we describe them here because, as we shall see later, they play an important role in the formation of complexes with DMSO. Two of them display an intramolecular NH…O H-bond, with the OH in axial position. They are almost isoenergetic and are higher in energy by 1.5-1.8 kcal mol^{-1} relative to the most stable OH…N form. They differ from each other by the orientation of the OH group, outwards the molecule in **eq**g^+G^-, and towards the aromatic ring in **eq**tG^-. The availability of the OH group for forming H-bonds is therefore expected to be different in the two forms.

TABLE 1 Relative Gibbs energy $\Delta(G)$ and ZPE corrected energy $\Delta(E_0)$ of the *cis*-AI monomers calculated in a DMSO PCM solvation continuum

The last three monomer geometries are **ax**g^-G^-, **eq**tG^+, and **ax**g^-T. They are higher in energy than the most stable form by 2.2, 2.4 and 3.0 kcal mol^{-1}, respectively, because they lack any intramolecular H-bonding interaction, which makes both OH and NH_2 groups available for interacting with the solvent. However, they differ in terms of expected interactions with the solvent by the fact that in **ax**g^-G^- one of the amino hydrogen atoms points inwards.

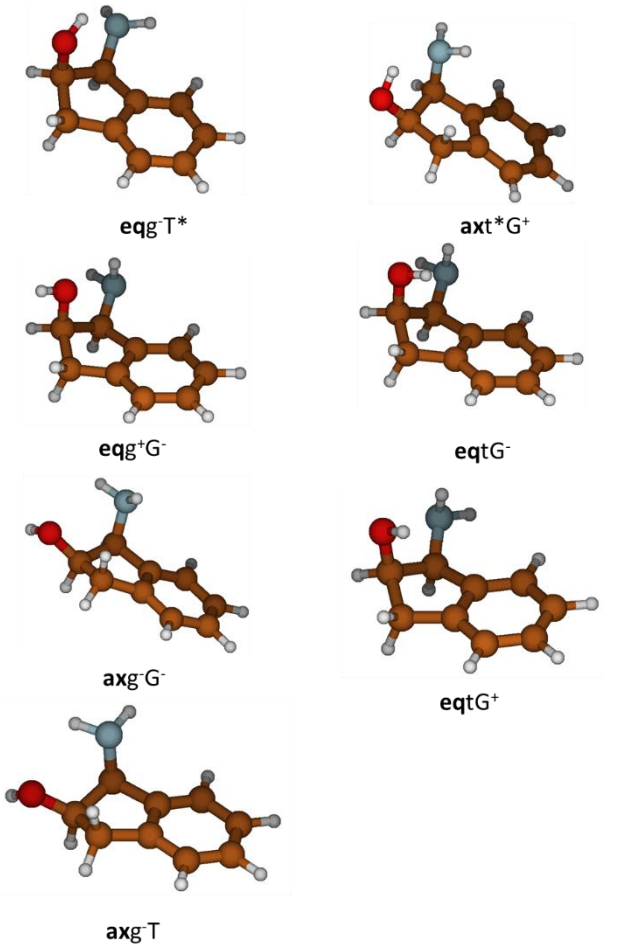


FIGURE 1 Structures of the (1*S*,2*R*)-*cis*-AI monomer in a DMSO solvent continuum

***cis*-AI:DMSO Complexes**

At the B3LYP/6-311++G(d,p) level of theory, five main conformers are populated. Their relative Gibbs energy is listed in Table 2 and the geometries are depicted in Figure 2.

TABLE 2 Relative Gibbs energy and ZPE corrected energy $\Delta(E_0)$ of the 1:1 *cis*-AI complexes with DMSO calculated in a DMSO PCM solvation continuum

In terms of ΔG, the most stable 1:1 complex, noHB-**eq**g⁻T*, contains the most stable monomer and is not H-bonded to the DMSO molecule. This structure is stabilized by keeping the intramolecular interaction intact and by favorable entropic effects due to its loose character. As discussed previously for the related system *trans*-AI, the remote position of the solvent might also be an artefact of the method that lacks dispersion correction.[46] Still, we will consider this structure in what follows, as a model of the *cis*-AI solute unperturbed by the interaction with the solvent and keeping its intramolecular H-bond intact. The second conformer, $mono_{OH}$-**eq**g⁺G⁻, involves an intermolecular OH…O H-bond, which is facilitated by the OH group pointing outward the aromatic ring. It contains a higher-energy conformer of the monomer with an intramolecular NH…O H-bond. The presence of both intra and intermolecular H-bonds, within the complex, stabilizes the **eq**g⁺G⁻ conformer due to cooperative effects. The third 1:1 complex, $mono_{NH}$-**eq**g⁻T*, is again based on the most stable conformer of *cis*-AI and displays a single intermolecular H-bond between the amino group of *cis*-AI and the oxygen atom of DMSO. Complexes involving a NH…O H-bond from the other NH group are much higher in energy at this level of theory. Then $mono_{OH}$-**ax**g⁻G⁻ is constructed on the **ax**g⁻G⁻ structure, which is very disfavored in the monomer due to the lack of H-bond. It is stabilized by an OH…O H-bond with the solvent. Finally, noHB-**ax**t*G⁺ is based on a stable OH…N geometry of the monomer. It is the **ax** counterpart of noHB-**eq**g⁻T* built on the most stable geometry and deserves the same comments. As Figure 2 shows, these five geometries have in common the fact that the DMSO molecule is relatively far from the aromatic ring.

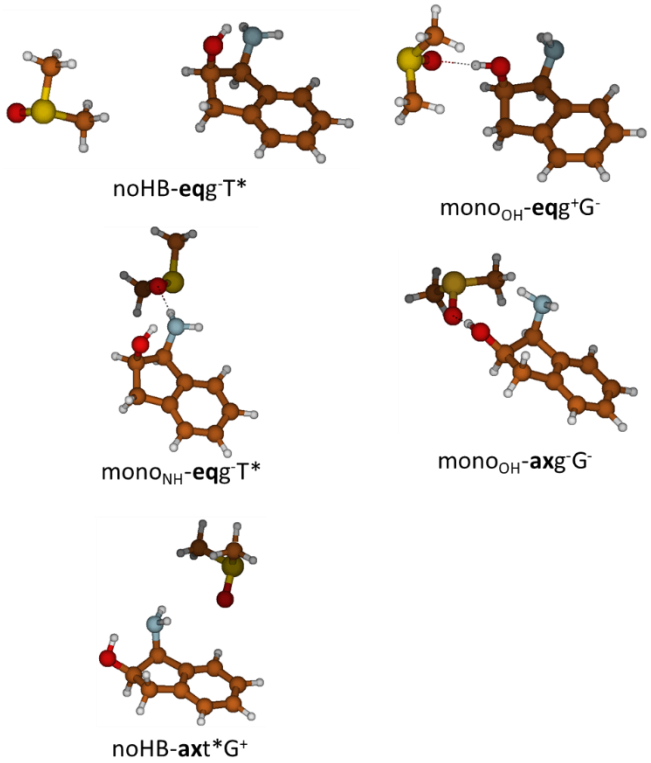


FIGURE 2 Structures of the 1:1 complexes of (1*S*,2*R*)-*cis*-AI with DMSO in a DMSO solvent continuum.

In contrast, only two 1:1 complexes are expected to be populated at the B3LYP-D3BJ/6-311++G(d,p) level of theory, monoOH-**eq**tG⁻ and bi-**eq**tG⁻ (Figure S1). monoOH-**eq**tG⁻ involves a single OH…O H-bond while a bifurcated H-bond takes place in bi-**eq**tG⁻, with simultaneous interaction between DMSO and the two protic groups. These complexes both contain the **eq**tG⁻ monomer, which has the OH dangling inwards. This geometry allows concomitant formation of an H-bond between OH and DMSO and a strong interaction between the solvent and the aromatic ring, the DMSO molecule lying above the latter. Structures involving strong dispersion interactions are strongly favored here.

It was reported in the literature that spectra simulations based on ZPE corrected energies ΔE_0 Boltzmann weights were in better agreement with the experiment than those predicted based on Gibbs free energies ΔG, because incorrect entropic factors resulting from intermolecular vibrations.[60] We therefore compared the two approaches. Table 2 lists the relative ΔE_0 of the 1:1 complexes. The stability order is very different from that obtained with ΔG. Only those involving an OH…O bond ($mono_{OH}$) are stable if one considers ΔE_0. This is because they are more strongly bound hence stiffer than $mono_{NH}$ or noHB complexes, thus disfavored when entropy is considered.

***cis*-AI:$DMSO_2$ Complexes**

The most stable 1-2 complexes are shown in Figure 3 and their relative Gibbs energies are given in Table 3. These complexes

all correspond to calculated 1:1 complexes whose structure is not modified by the addition of a second DMSO molecule. In contrast, the relative energies are strongly modified.

TABLE 3 Relative Gibbs energy and ZPE corrected energy $\Delta(E_0)$ of the 1:2 *cis*-AI complexes with DMSO calculated in a DMSO PCM solvation continuum

The most stable 1:1 complex noHB-**eq**g$^-$T* is destabilized by adding a second DMSO molecule, as is monoNH-**eq**g$^-$T*. In contrast, the complexes involving an OH…O H-bond like monoOH-**eq**g$^+$G$^-$, mono$_{OH}$-**eq**tG$^-$ or dmso-mono$_{OH}$-**ax**g$^-$T are stabilized by adding a second solvent molecule. The first 1:2 complex not derived from a 1:1 complex, namely, monoOH-monoNH-**eq**tG$^-$, is higher in energy by more than 5 kcal mol^{-1}. Including dispersion corrections considerably modifies the energy ordering (see Table 3). In particular, the complexes involving two interactions with the DMSO like monoOH-monoNH-**eq**tG$^-$ or dmso-bi-**eq**tG$^-$ are much stabilized. The geometry of the complexes is shown in Figure S1. The first three structures are built on the **eq**tG$^-$ conformer of *cis*-AI, already involved in the 1:1 complexes calculated at the same level. Among these structures, dmso-mono$_{OH}$-**eq**tG$^-$ and dmso-bi-**eq**tG$^-$ consist in adding a DMSO to the 1:1 complexes calculated at the same level. The third one, dmso-monoOH-eqtG$^+$ displays a single OH…O H-bond with the hydroxyl pointing inwards which allows a strong interaction between the DMSO and the aromatic ring. The fourth one, mono$_{OH}$-mono$_{NH}$-**eq**tG$^-$, involves simultaneous OH…O and NH…O H-bond formation with two different DMSO molecules. Like for the 1:1 complex, inclusion of dispersion correction favors these four geometries allowing the solvent to interact with the aromatic ring. The less stable calculated 1:2 complex is dmso-mono$_{OH}$-**ax**g$^-$G$^-$, for which the DMSO, linked to *cis*-AI through an intermolecular H-bond, is far from the aromatic ring.

We also compared the stability of the 1:2 complexes based on ΔE_0 (see Table 3). The stability ordering differs less from ΔG to ΔE_0 than for the 1:1 complex. Still, there are marked differences. When considering ΔE_0, all the stable complexes possess an OH…O hydrogen bond. The noHB complex is strongly destabilized while the bifurcated complex is stabilized, due to entropic reasons as mentioned for the 1:1 complex.

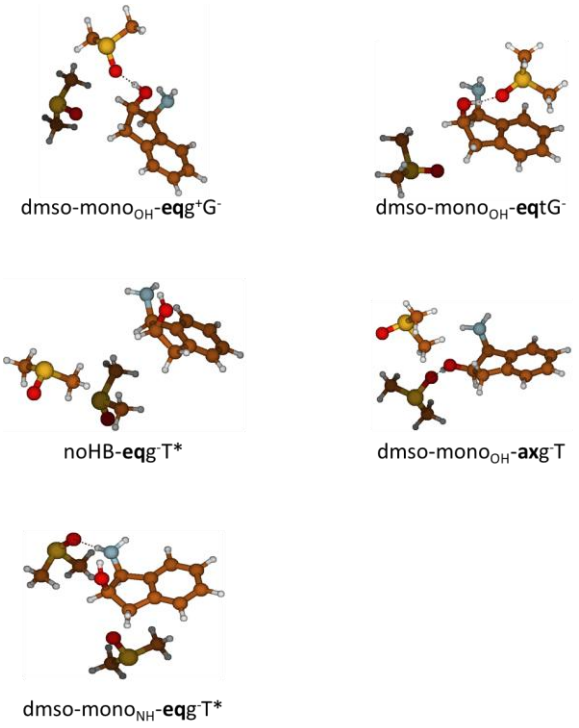


FIGURE 3 Structures of the 1:2 complexes of (1*S*,2*R*)-*cis*-AI with DMSO in a DMSO solvent continuum.

Spectral Assignment by Comparison with the Experiment

In this section, we will discuss the factors affecting the shape of the calculated VCD signal by comparing the simulated spectra to the experiment. The experimental VCD spectrum shown in Figure 4 is that of (1*S*,2*R*)-cis-AI obtained by taking the half difference between (1*S*,2*R*)-cis-AI and (1*R*,2*S*)-cis-AI. The raw spectra are shown in Figure S2 for the two enantiomers and display very satisfactory specular relation. The simulated spectra are constructed from the Boltzmann-averaged contributions based on the Gibbs energies of the structures with population larger than 5% at the B3LYP/6-311++G(d,p) level. We will discuss how the simulated spectra compare to the experiment for the monomer, as well as the complex with one or two solvent molecules. Special attention will be paid to the modes that are possibly involved in H-bonding interactions with the solvent like β(OH) at ~1400 cm^{-1}, β(NH$_2$) at ~ 1600 cm^{-1} and the NH$_2$ rocking motion in the 1200 cm^{-1} range. We will also discuss how dispersion corrections and entropic factors affect the relative weight of the structures.

Isolated Molecule

The Boltzmann-averaged IR and VCD spectra of the monomer, based on either ΔG or ΔE_0, together with the spectra of the individual conformers, are compared to the experiment in Figure 4. The simulated IR spectrum is in good agreement with the experiment below 1300 cm^{-1} and above 1430 cm^{-1}. However, the region between 1300 and 1430 cm^{-1} shows strong discrepancy between the two spectra. This region contains the β(OH) and delocalized bending modes with a strong contribution of the OH bend, which are expected to be sensitive to molecular interactions. Although the comparison between calculated and simulated intensities should be taken with caution, due to different band widths, it clearly appears that the calculated relative intensity of the transitions at 1406 and 1387 cm^{-1} is too high relative to the rest of the spectrum. In addition, the feature calculated at 1353 cm^{-1} is blue shifted compared to the experiment. The mismatch between calculated and experimental

VCD spectra is even more explicit. The band calculated at 1612 cm^{-1}, in the region of the β(NH), is negative while it is a bisignate with a large positive contribution in the experimental spectrum. The negative features observed at 1434 and 1256 cm^{-1} have no counterparts in the calculated spectrum. Conversely, the very strongly negative calculated band at 1353 cm^{-1} is not observed. Only the transitions at 1380 and 1192 cm^{-1} seem to be well simulated. It can be deduced from the individual contribution spectra that these two transitions arise from the most stable **eq**g$^-$T* conformer. Moreover, the bisignate signature at 1612 cm^{-1} is neither accounted for by the **eq**g$^-$T* nor by the **ax**tG$^+$ conformers. As the relative energies of the most stable conformers are almost identical at B3LYP and B3LYP-D3BJ levels, the resulting averaged IR and VCD spectra (not shown) are the same with the two methods. Replacing ΔG by ΔE_0 does not modify the spectrum substantially either as entropic effects are not important in the monomer.

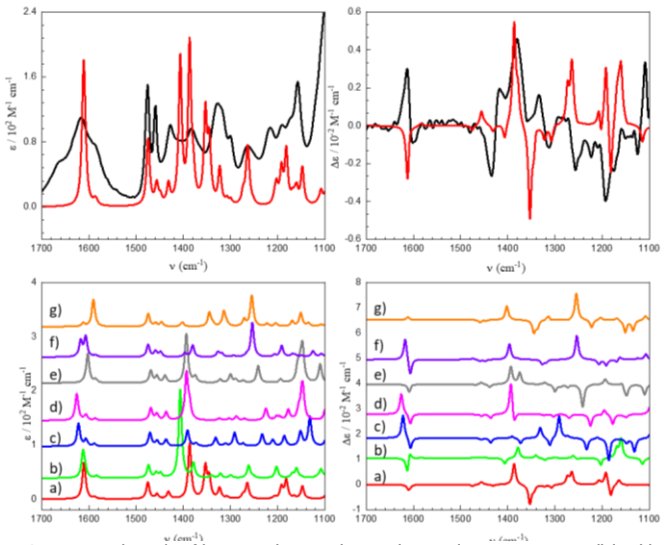


FIGURE 4 (Top/Left) Experimental IR absorption spectrum (black) compared with the simulated spectrum based on the Boltzmann-averaged contributions of the monomers, with ΔG calculated at the B3LYP/6-31G++(d,p) level (red). (Top/Right) Same for the VCD spectrum. (Bottom/Left) Individual IR contributions calculated at the B3LYP/6-311G++(d,p) level. (Bottom/Right) Same for VCD. a) **eq**g$^-$T*, b) **ax**tG$^+$, c) **eq**g$^+$G$^-$, d) **eq**tG$^-$, e) **eq**tG$^+$, f) **ax**g$^-$G$^-$, g) **ax**g$^-$T.

1:1 Complexes

The IR and VCD spectra averaged over the five most stable structures are given in Figure 5. The agreement is considerably improved relative to the monomer, for both IR and VCD signals. The only flaw in the IR spectrum is the slight overestimation of the relative intensity of the β(OH) transition at 1387 cm^{-1}. The VCD spectrum is now satisfactory; in particular the bisignate signal observed at 1612 cm^{-1} is well accounted for in the simulation. The main discrepancy is observed for the transition calculated at 1353 cm^{-1}, which is too negative compared to the experimental spectrum, as it was in the VCD spectrum simulated for the monomer.

The individual contributions to the VCD spectrum are given in Figure 5 (bottom). The most stable family of complexes, noHB-**eq**g$^-$T*, contributes up to 60% to the average. Due to the lack of specific interaction with the solvent, it displays the same spectrum as the parent monomer, with no bisignate signal and by far too negative a feature at 1353 cm^{-1}. The high contribution of this complex explains the mismatch mentioned above. The VCD spectrum of mono$_{OH}$-**eq**g$^+$G$^-$, which contributes by 26%, is strongly modified compared to the parent monomer and matches the experiment much better. In the 1600 cm^{-1} range however, very little modification is observed. The bisignate is well reproduced, as it was in the **eq**g$^+$G$^-$ monomer, and is associated with the G$^-$ orientation of the NH_2 group. As already described for *trans*-AI,[46] the positive signal corresponds to pure NH_2 scissoring motion, while the negative signal is due to scissoring of the NH_2 group strongly coupled with the aromatic CH bending motions. In contrast, the pattern between 1380 and 1420 cm^{-1}, assigned to coupled bending motions involving β(OH) is strongly modified relative to the parent monomer. The two negative VCD features in the 1420-1440 range correspond to the H-bonded β(OH) coupled with the β(CH_2). The interaction with DMSO results in both an upshift in frequency and a change in the description of the modes in terms of motions of the nuclei, which were described in terms of coupled β(OH) and β(C_1H) motions in the monomer. The VCD signal is more negative in the complex than in the monomer, which reproduces well the negative feature experimentally observed at ~1440 cm^{-1}. The 1200 cm^{-1} region (NH_2 rocking motion) is also modified. While the NH_2 rocking motion is well isolated from the other modes in the monomer and appears at 1185 cm^{-1} as a single strongly negative signal in the VCD spectrum, three modes can be described in terms of NH_2 rocking motion combined with ring deformations or CH bends in the complex. This leads to the three negative bands calculated in the 1200 cm^{-1} range. These observations are the signature of the formation of the intermolecular OH…O H-bond at the detriment of the intramolecular interaction. Nevertheless two bands are still at odd with the experimental spectrum, a negative signal at 1420 and a positive signal at 1300 cm^{-1}. These modes can be described, like before, in terms of modes involving the OH bend motion. The spectrum of mono$_{NH}$-**eq**g$^-$T* is not strongly modified by the NH…O interaction. Therefore, its calculated spectrum resembles that of noHB- **eq**g$^-$T* and does not match the experiment. The last contributing complex is mono$_{OH}$-**ax**g$^-$G$^-$. Its spectrum does not match the experiment well as it shows a strong positive signal at ~1300 cm^{-1}, assigned to a mode strongly modified by complexation because it involves the OH bend that gains VCD activity via complexation. There is little consequence on the quality of the spectrum due to its limited contribution (5 %). The remaining complexes, noHB-axt*G+, monoOH-axg-T, monoOH-eqtG-, bi-eqtG- and monoNH-axt*G+, do not contribute to the averaged spectrum.

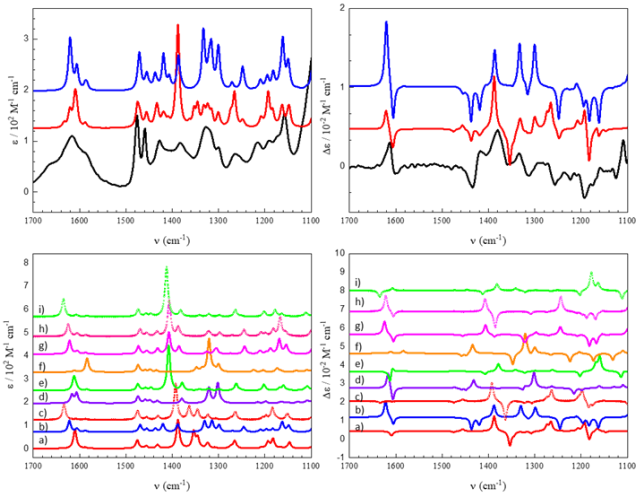


FIGURE 5 (Top/left) Experimental IR absorption spectrum (black) compared with the simulation resulting from Boltzmann averaged contribution of the 1:1 complexes calculated at the B3LYP/6-311G++(d,p) level using ΔG (red) or ΔE_0 (blue).(Top/Right) Same for the VCD spectrum. (Bottom/Left) Individual IR contributions calculated at the B3LYP/6-311G++(d,p) level. (Bottom/Right) Same

for VCD. a) noHB-**eq**g$^-$T*, b) monoOH-**eq**g$^+$G$^-$, c) monoNH-**eq**g.T*, d) monoOH-**ax**g$^-$G$^-$, e) noHB-**ax**t*G$^+$, f) monoOH-**ax**g$^-$T, g) monoOH-**eq**tG$^-$, h) bi-**eq**tG$^-$, i) monoNH-**ax**t*G$^+$. Note that the spectra with identical colors correspond to structures containing identical monomers

The results obtained at the B3LYP-D3BJ/6-311++G(d,p) level are given in Figure 6. The Boltzmann-averaged VCD spectrum, based on 86% of the mono$_{OH}$-**eq**tG$^-$ and 14% of the bi-**eq**tG$^-$ conformers, shows decent agreement below 1300 cm^{-1} and above 1430 cm^{-1} but, as already noticed for the monomer, the 1300 - 1430 cm^{-1} region is at odd with the experiment. As discussed previously, the G$^-$ configuration of the amino group accounts well for the bisignate signature at 1612 cm^{-1}. Nevertheless, the **eq**t geometry of the hydroxyl group where the hydroxyl group point to the aromatic ring seems to be responsible for the discrepancy in the central region of the spectrum. The negative peaks observed instead of positive ones at 1329 and 1387 cm^{-1} are due to β(OH) coupled with β(C$_1$H) and β(OH) coupled with the NH$_2$ rocking motion in the monoOH-**eq**tG$^-$ and bi-**eq**tG$^-$, respectively. Moreover, a positive transition is observed at 1250 cm^{-1} where a negative feature is expected. This band arising from both complexes is attributed to β(OH) coupled with β(CH) localized on the 5-member ring. This observation suggests that complexes with the DMSO located over the aromatic ring do not account well for the experimental results. Moreover, as discussed in the case of the B3LYP results, the most affected regions are those where modes involving OH bending motions appear. When using ΔE_0 instead of ΔG for simulating the spectrum (Figure 6), the agreement between simulated and experimental spectra is acceptable in terms of band position. However some discrepancies are met in the relative intensities. The bisignate at ~1600 cm^{-1} and the two positive bands at ~1300 cm^{-1} are too intense compared to the rest of the spectrum. This can be explained the exclusive contribution of complexes with an OH…O H-bond, in particular too large a contribution of mono$_{OH}$-**ax**g$^-$G$^-$.

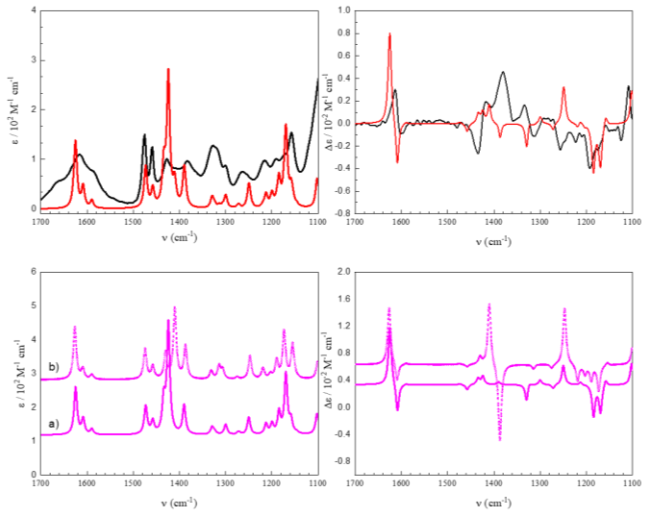


FIGURE 6 (Top/Left) Experimental IR absorption spectrum (black) compared with the simulation resulting from Boltzmann averaged contribution of the 1:1 complexes calculated at the B3LYP-D3BJ/6-311G++(d,p) level taking into account ΔG (red). (Top/Right) Same for the VCD spectrum. (Bottom/Left) Individual IR contributions calculated at the same level. (Bottom/Right) Same for VCD. a) monoOH-**eq**tG$^-$, b) bi-**eq**tG$^-$. Identical colors correspond to structures containing identical monomers.

1:2 Complexes The simulated IR absorption and VCD spectra are given in Figure 7 together with the experiment and the individual contributions. Both IR and VCD spectra match the experimental results very well. The relative IR absorption is satisfactory on the whole spectrum, in particular at 1387 cm^{-1} where it was overestimated for the monomer and the 1:1 complex. Regarding the VCD spectrum, the intensity and sign are well reproduced at 1353 cm^{-1} where the monomer and the 1:1 complex were at odd with the experiment. The only minor discrepancy is at 1417 cm^{-1} where a weak negative signal is calculated instead of the weak positive signal expected.

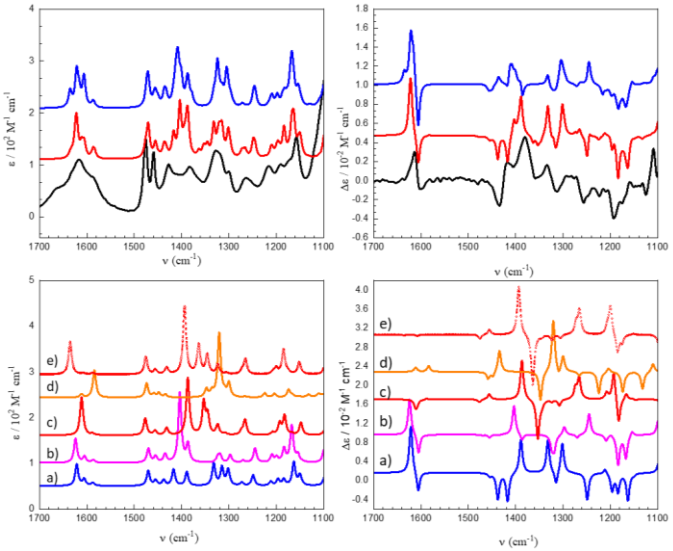


FIGURE 7 (Top/left) Experimental IR absorption spectrum (black) compared with the simulation resulting from Boltzmann averaged contributions of the 1:2 complexes calculated at the B3LYP/6-311G++(d,p) level, using ΔG (red) or ΔE (blue). (Top/Right) Same for the VCD spectrum. (Bottom/Left) Individual IR contributions calculated at the same level of theory. (Bottom/Right) Same for VCD. a) dmso-monoOH-**eq**g$^+$G$^-$, b) dmso-monoOH-**eq**tG., c) noHB-**eq**g.T*; d) dmso-monoOH-**ax**g.T; e) dmso-monoNH-**eq**g$^-$T*. Identical colors correspond to structures containing identical monomers.

The most stable complex dmso-monoOH-**eq**g$^+$G$^-$, with population of 48%, is already in good agreement with the experiment. Its VCD spectrum is not modified relative to the monoOH-**eq**g$^+$G$^-$ 1:1 complex from which it is derived (see 5). This geometry is responsible for the discrepancy at 1417, as it was in the 1:1 complex. The second most stable 1:2 complex, dmso-monoOH-**eq**tG$^-$, contributes by 26%. In terms of band position and shape, this complex is compatible with the experiment and can contribute to the VCD spectrum. Finally, the other calculated 1:2 complexes, no$_{HB}$-**eq**g$^-$T*, dmso-mono$_{OH}$-**ax**g$^-$T and dmso-mono$_{NH}$-**eq**g$^-$T*, contribute by a lesser extent to the average. Having the amino group in T or T* conformation, they do not display the bisignate signal attributed to G$^-$. It should be noted that the contribution of the complexes built on **eq**g$^-$T* is less than for the monomer or the 1:1 complex, which explains the better agreement.

The results obtained at the B3LYP-D3BJ/6-311++G(d,p) level are given in Figures 8. They lead to similar conclusions as for their 1:1 homologues, due to similar contributions, namely, 70 % of dmso-mono$_{OH}$-**eq**tG$^-$, 22% of dmso-bi-**eq**tG$^-$ and 8% of mono$_{OH}$-mono$_{NH}$-**eq**tG$^-$. The experiment is well accounted for above 1500 cm^{-1} and below 1230 cm^{-1}. In between, the discrepancies are the same as those observed for the 1:1 complex and arise from the same reasons.

Finally, the spectrum constructed using Boltzmann contributions calculated from ΔE_0 is completely at odd with the experiment (see Figure 7). This is due to the fact that using ΔE_0 favors tight

complexes, in particular the bifurcated dmso-bi-**eq**tG$^-$ and the bisolvated mono$_{OH}$-mono$_{NH}$-**eq**tG$^-$, whose spectrum does not reproduce the experiment.

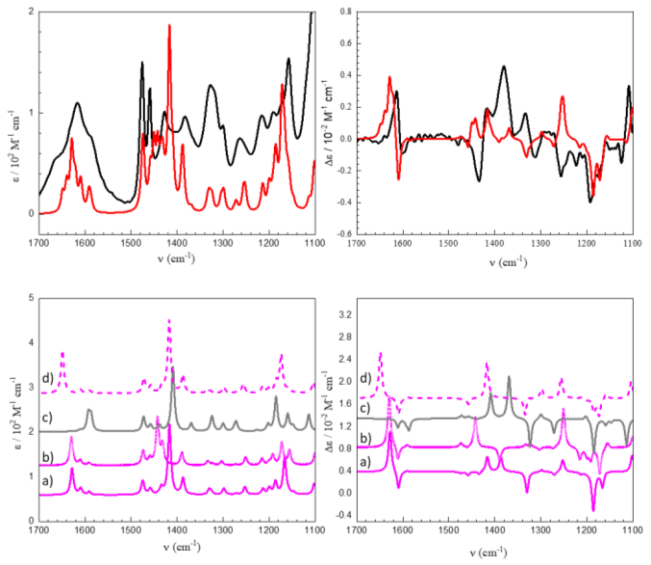


FIGURE 8 (Top/left) Experimental IR absorption spectrum (black) compared with the simulation resulting from Boltzmann averaged contribution of the 1:2 complexes calculated at the B3LYP-D3BJ/6-311G++(d,p) level using ΔG (red). (Top/Right) Same for the VCD spectrum. (Bottom/Left) Individual IR contributions calculated at the same level. (Bottom/Right) Same for VCD. a) dmso-monoOH-**eq**tG$^-$, b) dmso-bi-**eq**tG$^-$, c) dmso-monoOH-**eq**tG$_+$, d) monoOH-monoNH-**eq**tG$^-$. Identical colors correspond to structures containing identical monomers.

DISCUSSION

Role of Solvation

Solvation has two major effects. It first affects the relative energy of the different conformers. Second, for a given structure, it may result in modifications of the spectrum. The latter point appears clearly from the comparison of the solute spectra in the monomer, 1:1, and 1:2 complexes, shown in Figures 4, 5, and 7. The main modifications in terms of frequencies, intensities, and for the VCD spectra, sign of the peaks, are due to the addition of the first solvent molecule, mainly on the OH group of *cis*-AI. As expected, complexation mostly affects the modes depicted in terms of OH bending motions.

Changes in relative Gibbs energies are already brought by the first molecule of solvent. However, further changes, which result in an improvement of the agreement between experiment and simulation, is brought by the second solvent molecule. To check this hypothesis, a simulated VCD spectrum built from the individual contributions of the 1:1 complexes weighted by the Boltzmann contributions of the corresponding 1:2 complexes is shown in Figure S3. The spectrum built from the 1:1 complexes is almost identical to that of the 1:2 complex. This shows that the second solvent molecule mainly contributes via the energy ordering, and does not result in spectral modifications.

The second question concerning solvation is whether the H-bond opening has a signature in the VCD spectrum. The intramolecularly bonded geometries (**eq**g$^-$T* and **ax**t*G$^+$) are characterized by a very intense β(OH) in the IR absorption, which results in the mismatch observed at ~1400 cm^{-1} in the IR absorption simulated with the Boltzmann average of the monomers or the 1:1 complex, resulting from too high a contribution of these conformers. We can conclude that non-intermolecularly H-bonded structures cannot contribute strongly to the spectrum. This is what is expected from chemical considerations in the full solvation limit. The signature of the intermolecular H-bond appears in both the IR absorption and VCD spectra. As can be expected, the most affected region is that containing modes involving the β(OH) motion in the region of 1400 cm^{-1}. For **eq**g$^+$G$^-$, which displays no intramolecular H-bond in the monomer, the β(OH) is blue shifted upon formation of the intermolecular H-bond and its VCD signal changes sign. In contrast, the NH_2 scissoring motion is not much affected when the interaction is located on the OH group. The G$^-$ structures keep their characteristic bisignate signature whether interacting or not with DMSO *via* the OH group. Interaction with the NH_2 group does not modify much the VCD and IR spectra either, apart from a blue shift of the band in the 1600 cm^{-1} region. Last, we can compare similar geometries, namely **eq**tG$^-$ and **eq**g$^+$G$^-$ that only differ by the rotation of the OH group, inwards for the former and outwards for the latter. The spectrum of **eq**tG$^-$ is clearly at odd with the experiment below 1400 cm^{-1}. By forcing the OH group to rotate outside to allow H-bond formation, the solvent improves the agreement with the experiment. Last, for a given H-bonded structure, modifying the puckering angle has strong consequences. As shown in Figure 4, the VCD spectra of **eq**g$^-$T* and **ax**t*G$^+$ bear little resemblance. The presence of one or two DMSO molecule also allows favoring the **eq** conformers, which match the experiment better.

Effect of Dispersion Corrections

The dispersion corrections are known to be necessary to satisfactorily reproduce the structure of gas-phase clusters.[61] In the cluster-in-the-liquid limit, the dispersion corrections overestimate the structures with the solvent interacting with the aromatic ring, which would be probably more adapted to gas-phase clusters of limited size and are not representative of full solvation.[46] The conclusion that dispersion is overestimated when describing the VCD spectra of aromatic chiral acids in the very same DMSO solvent has been drawn already by Bünnemann and Merten.[62] This kind of folded structure forces a rotation of the protic substituent inwards. As discussed above, this results in a less satisfactory match with the experiment.

Effect of Entropy

The effects of entropy can be assessed by comparing the simulated spectrum using Boltzmann weights resting on ΔE_0 or ΔG. Using ΔG leads to the overestimated contribution of very floppy complexes, like those with no H-bond with the solvent that are not physically relevant. However, this weakness is corrected when using 1:2 complexes. The presence of a second DMSO molecule is sufficient for reproducing the spectrum. In contrast, using ΔE_0 results to overestimated contribution of rigid complexes. For the 1:1 complex, only those showing an OH…O bond to the solvents contribute to the spectrum, which gives a physically relevant picture of the main interaction at play in this system. However, the situation deteriorates when going to the 1:2 complex. The simulated VCD spectrum is in this case completely at odd with the experiment, because of the overestimated contribution of rigid structures like the bifurcated complex.

The effect of entropy can also be assessed by comparing the spectra of Figures 5 and 7, obtained from the weighted average of all the conformational variants obtained for each family, with those considering only the most stable geometry of each family (Figures S4 and S5 of the SI). The latter approach was used successfully by the groups of Xu and Merten, with the weights of

the different clusters obtained by adjustment to the experimental VCD spectrum.[63,64]

Comparison with other indan Derivatives

We shall finally compare *cis*-AI with similar systems in DMSO like 1-indanol[37] or *trans*-AI.[46] Like for 1-indanol, the OH bend region displays a clear signature of solvation by DMSO, both in terms of band position and VCD signature. Besides the modification brought by the H-bond formation, solvation forces the OH group to rotate outside the molecular frame, which results in a better agreement with the experiment. Although *cis*-AI displays an intramolecular H-bond and *trans*-AI does not, the two molecules show similarities. In both systems, a bisignate signature is experimentally observed at ~1600 cm^{-1} and is only accounted for by considering G^- structures. In both systems, the complexes involving a single H-bond between OH and DMSO play a major role. The bifurcated 1:1 complexes are dominant in *trans*-AI because the *trans* position of the two substituents allows easy insertion of the solvent. In contrast, they are calculated very high in free energy in *cis*-AI because they demand the DMSO insert in the intramolecular H-bond, which does not make the H-bond optimal due to steric constrains. Bifurcated 1:1 complexes are stabilized when including dispersion, but again they contain monomers with OH directed inwards, which is not satisfactory in terms of agreement with the experiment.

Conclusion

We have studied the VCD spectrum of *cis*-AI in DMSO in the frame of the cluster-in-the-liquid model. Two DMSO molecules are sufficient for a satisfactory match with the experiment. The first DMSO molecule modifies the spectrum relative to the monomer, while the second DMSO adjusts the Boltzmann contributions. The conformers, which reproduce well the spectrum, do not have intramolecular H-bond. OH must be outside (*i.e.* DMSO far from the aromatic ring) and interact with the solvent. These conformers are found when no dispersion is included, which underlines the limits of the cluster-in-the-liquid model, which is far from full solvation. However, satisfactory agreement between experiment and simulation is obtained at a reduced computational cost. This system also illustrates that entropic effects are a bottleneck in the cluster-in-the-liquid model: while using ΔG tends to overestimate the contribution of very floppy systems, using ΔE_0 overestimates the contribution of rigid systems. This approach also allows us to find transferable parameters like the bisignate signature at ~1600 cm^{-1} that is the signature of the G^- conformation of the NH substituent in indan derivatives. Further work is in progress on the VCD signature of the solid-state structure of this class of molecules.

Acknowledgements

We thank Anaël Danielou for experimental assistance. This work has been supported by the French National Research Agency (ANR) Dichroprobe project (Grant ANR-18-CE29-0001-01). We acknowledge computer time allowances by DSI Université Paris Saclay and the use of the computing facility cluster MésoLUM of the LUMAT federation (FR LUMAT 2764).

Supporting information

Additional supporting information may be found in the online version of this article at the publisher's website. It contains Figures S1 to S5 as well as the xyz coordinates of the discussed structures.

REFERENCES AND NOTES

1. Steiner S, Desiraju GR. The Weak Hydrogen Bond. Oxford: Oxford University Press; 1999.
2. Kabsch W, Sander C. Dictionary of protein secondary structure - pattern-recognition of hydrogen-bonded and geometrical features. *Biopolymers* **1983**;22:2577-2637.
3. Brenner V, Gloaguen E, Mons M. Rationalizing the diversity of amide-amide H-bonding in peptides using the natural bond orbital method. *Physical Chemistry Chemical Physics* **2019**;21:24601-24619.
4. Schwing K, Gerhards M. Investigations on isolated peptides by combined IR/UV spectroscopy in a molecular beam - structure, aggregation, solvation and molecular recognition. *International Reviews in Physical Chemistry* **2016**;35:569-677.
5. Altnoeder J, Lee JJ, Otto KE, Suhm MA. Molecular Recognition in Glycolaldehyde, the Simplest Sugar : two isolated Hydrogen Bonds Win Over One Cooperative Pair. *ChemistryOPEN* **2012**;1:269-275.
6. Borho N, Suhm MA, Le Barbu-Debus K, Zehnacker A. Intra- vs. intermolecular hydrogen bonding: dimers of alpha-hydroxyesters with methanol. *Physical Chemistry Chemical Physics* **2006**;8:4449-4460.
7. Zehnacker A. Chirality Effects in Gas-Phase Spectroscopy and Photophysics of Molecular and Ionic Complexes: Contribution of Low and Room Temperature Studies. *International Reviews in Physical Chemistry* **2014**;33:151-207.
8. Seurre N, Sepiol J, Le Barbu-Debus K, Lahmani F, Zehnacker-Rentien A. The role of chirality in the competition between inter and intramolecular hydrogen bonds: jet-cooled van der Waals complexes of (+/-)2-naphthyl-1-ethanol with (+/-)1-amino-2-propanol and (+/-)2-amino-1-butanol. *Physical Chemistry Chemical Physics* **2004**;6:2867-2877.
9. Butz P, Kroemer RT, Macleod NA, Simons JP. Hydration of neurotransmitters: a spectroscopic and computational study of ephedrine and its diastereoisomer pseudoephedrine. *Physical Chemistry Chemical Physics* **2002**;4:3566-3574.
10. Le Barbu-Debus K, Broquier M, Mahjoub A, Zehnacker-Rentien A. Chiral recognition in jet-cooled complexes of (1R,2S)-(+)-cis-1-amino-2-indanol and methyl lactate: on the importance of the CH center ...p interaction. *Physical Chemistry Chemical Physics* **2009**;11:7589-7598.
11. Macleod NA, Simons JP. Neurotransmitters in the gas phase: Infrared spectroscopy and structure of protonated ethanolamine. *Physical Chemistry Chemical Physics* **2004**;6:2821-2826.
12. Bouchet A, Klyne J, Ishiuchi S-i, Dopfer O, Fujii M, Zehnacker A. Stereochemistry-dependent structure of hydrogen-bonded protonated dimers: the case of 1-amino-2-indanol. *Physical Chemistry Chemical Physics* **2018**;20:12430-12443.
13. Le Barbu-Debus K, Guchhait N, Zehnacker-Rentien A. Electronic and infrared spectroscopy of jet-cooled (+/-)-cis-1-amino-indan-2-ol hydrates. *Physical Chemistry Chemical Physics* **2007**;9:4465-4471.
14. Asselin P, Madebene B, Soulard P, Georges R, Goubet M, Huet TR, Pirali O, Zehnacker-Rentien A. Competition between inter- and intra-molecular hydrogen bonding: An infrared spectroscopic study of jet-cooled amino-ethanol and its dimer. *Journal of Chemical Physics* **2016**;145.
15. Graham RJ, Kroemer RT, Mons M, Robertson EG, Snoek LC, Simons JP. Infrared ion dip spectroscopy of a noradrenaline analogue: Hydrogen bonding in 2-amino-1-phenylethanol and its singly hydrated complex. *Journal of Physical Chemistry A* **1999**;103:9706-9711.
16. Cacela C, Fausto R, Duarte ML. A combined matrix-isolation infrared spectroscopy and MO study of 1-amino-2-propanol. *Vibrational Spectroscopy* **2001**;26:113-131.
17. Magyarfalvi G, Tarczay G, Vass E. Vibrational circular dichroism. *Wiley Interdisciplinary Reviews-Computational Molecular Science* **2011**;1:403-425.
18. Kawamura I, Sato H. Solid-state vibrational circular dichroism studies of L- and D-serine. *Analytical Biochemistry* **2019**;580:14-20.
19. Rode JE, Lyczko K, Jawiczuk M, Kawecki R, Stanczyk W, Jaglinska A, Dobrowolski JC. The Vibrational Circular Dichroism Pattern of the (C=O) Bands in Isoindolinones. *Chemphyschem* **2018**;19:2411-2422.
20. Perez-Mellor A, Zehnacker A. Vibrational circular dichroism of a 2,5-diketopiperazine (DKP) peptide: Evidence for dimer formation in cyclo LL or LD diphenylalanine in the solid state. *Chirality* **2017**;29:89-96.
21. Declerck V, Perez-Mellor A, Guillot R, Aitken DJ, Mons M, Zehnacker A. Vibrational circular dichroism as a probe of solid-state organisation of derivatives of cyclic beta-amino acids: Cis- and trans-2-aminocyclobutane-1-carboxylic acid. *Chirality* **2019**;31:547-560.
22. Tarczay G, Magyarfalvi G, Vass E. Towards the determination of the absolute configuration of complex molecular systems: Matrix isolation vibrational circular dichroism study of (R)-2-amino-1-propanol. *Angewandte Chemie-International Edition* **2006**;45:1775-1777.
23. Tarczay G, Gobi S, Vass E, Magyarfalvi G. Model peptide-water complexes in Ar matrix: Complexation induced conformation change and chirality transfer. *Vibrational Spectroscopy* **2009**;50:21-28.
24. Beke T, Somlai C, Magyarfalvi G, Perczel A, Tarczay G. Chiral and Achiral Fundamental Conformational Building Units of beta-Peptides: A Matrix Isolation Conformational Study on Ac-beta-HGly-NHMe and Ac-beta-HAla-NHMe. *Journal of Physical Chemistry B* **2009**;113:7918-7926.
25. Perera AS, Cheramy J, Poopari MR, Xu Y. Aggregation of lactic acid in cold rare-gas matrices and the link to solution: a matrix isolation-vibrational circular dichroism study. *Physical Chemistry Chemical Physics* **2019**;21:3574-3584.
26. Merten C, Xu Y. Chirality Transfer in a Methyl Lactate-Ammonia Complex Observed by Matrix-Isolation Vibrational Circular Dichroism Spectroscopy. *Angewandte Chemie-International Edition* **2013**;52:2073-2076.
27. Gobi S, Vass E, Magyarfalvi G, Tarczay G. Effects of strong and weak hydrogen bond formation on VCD spectra: a case study of 2-chloropropionic acid. *Physical Chemistry Chemical Physics* **2011**;13:13972-13984.
28. Buffeteau T, Cavagnat D, Bouchet A, Brotin T. Vibrational absorption and circular dichroism studies of (-)-camphanic acid. *Journal of Physical Chemistry A* **2007**;111:1045-1051.
29. Poopari MR, Zhu P, Dezhahang Z, Xu Y. Vibrational absorption and vibrational circular dichroism spectra of leucine in water under different pH conditions: Hydrogen-bonding interactions with water. *Journal of Chemical Physics* **2012**;137:194308.
30. Quesada-Moreno MM, Aviles-Moreno JR, Lopez-Gonzalez JJ, Claramunt RM, Lopez C, Alkorta I, Elguero J. Chiral self-assembly of enantiomerically pure (4.5,7R)-campho 2,3-c pyrazole in the solid state: a vibrational circular dichroism (VCD) and computational study. *Tetrahedron-Asymmetry* **2014**;25:507-515.
31. Jähnigen S, Scherrer A, Vuilleumier R, Sebastiani D. Chiral Crystal Packing Induces Enhancement of

Vibrational Circular Dichroism. *Angewandte Chemie-International Edition* **2018**;57:13344-13348.
32. Xia Y, Koenis MAJ, Collados JF, Ortiz P, Harutyunyan SR, Visscher L, Buma WJ, Nicu VP. Regional Susceptibility in VCD Spectra to Dynamic Molecular Motions: The Case of a Benzyl -Hydroxysilane. *Chemphyschem* **2018**;19:561-565.
33. Orestes E, Bistafa C, Rivelino R, Canuto S. Including Thermal Disorder of Hydrogen Bonding to Describe the Vibrational Circular Dichroism Spectrum of Zwitterionic L-Alanine in Water. *Journal of Physical Chemistry A* **2015**;119:5099-5106.
34. Kwac K, Lee KK, Han JB, Oh KI, Cho M. Classical and quantum mechanical/molecular mechanical molecular dynamics simulations of alanine dipeptide in water: Comparisons with IR and vibrational circular dichroism spectra. *Journal of Chemical Physics* **2008**;128:105106
35. Scherrer A, Vuilleumier R, Sebastiani D. Vibrational circular dichroism from ab initio molecular dynamics and nuclear velocity perturbation theory in the liquid phase. *The Journal of Chemical Physics* **2016**;145:084101.
36. Scherrer A, Vuilleumier R, Sebastiani D. Nuclear Velocity Perturbation Theory of Vibrational Circular Dichroism. *Journal of Chemical Theory and Computation* **2013**;9:5305-5312.
37. Le Barbu-Debus K, Scherrer A, Bouchet A, Sebastiani D, Vuilleumier R, Zehnacker A. Effect of puckering motion and hydrogen bond formation on the vibrational circular dichroism spectrum of a flexible molecule: the case of (S)-1-indanol. *Physical Chemistry Chemical Physics* **2018**;20:14635-14646.
38. Yang G, Xu Y. Probing chiral solute-water hydrogen bonding networks by chirality transfer effects: A vibrational circular dichroism study of glycidol in water. *Journal of Chemical Physics* **2009**;130:164506.
39. Losada M, Xu YJ. Chirality transfer through hydrogen-bonding: Experimental and ab initio analyses of vibrational circular dichroism spectra of methyl lactate in water. *Physical Chemistry Chemical Physics* **2007**;9:3127-3135.
40. Perera AS, Thomas J, Poopari MR, Xu YJ. The Clusters-in-a-Liquid Approach for Solvation: New Insights from the Conformer Specific Gas Phase Spectroscopy and Vibrational Optical Activity Spectroscopy. *Frontiers in Chemistry* **2016**;4:9.
41. Bünnemann K, Merten C. Solvation of N,C-Protected Valine: Interactions with DMSO and a Chiral Solvating Agent. *Journal of Physical Chemistry B* **2016**;120:9434-9442.
42. Bouchet A, Klyne J, Piani G, Dopfer O, Zehnacker A. Diastereo-Specific Conformational Properties of Neutral, Protonated and Radical Cation Forms of (1R,2S)-cis and (1R,2R)-trans Amino-Indanol by Gas Phase Spectroscopy. *Physical Chemistry Chemical Physics* **2015**;17:25809-25821.
43. Le Barbu-Debus K, Lahmani F, Zehnacker-Rentien A, Guchhait N. Electronic and infrared spectroscopy of chiral (+/-)-cis-1-amino-indan-2-ol in a supersonic jet. *Chemical Physics Letters* **2006**;422:218-225.
44. Johnson JL, Polavarapu PL. Chiral Molecular Structures of Substituted Indans: Ring Puckering, Rotatable Substituents, and Vibrational Circular Dichroism. *Acs Omega* **2019**;4:4963-4976.
45. Fontana LP, Chandramouly T, Smith HE, Polavarapu PL. Vibrational circular-dichroism and absolute-configuration of 1-substituted indans. *Journal of Organic Chemistry* **1988**;53:3379-3381.
46. Le Barbu-Debus K, Bowles J, Jahnigen S, Clavaguera C, Calvo F, Vuilleumier R, Zehnacker A. Assessing cluster models of solvation for the description of vibrational circular dichroism spectra: synergy between static and dynamic approaches. *Physical chemistry chemical physics : PCCP* **2020**;22:26047-26068.
47. Demarque DP, Merten C. Intra- versus Intermolecular Hydrogen Bonding: Solvent-Dependent Conformational Preferences of a Common Supramolecular Binding Motif from (HNMR)-H-1 and Vibrational Circular Dichroism Spectra. *Chemistry-a European Journal* **2017**;23:17915-17922.
48. Polavarapu PL, Santoro E, Covington CL, Johnson JL, Puente AR, Schley ND, Kallingathodi Z, Prakasan PC, Haleema S, Thomas AA and others. How important are the intermolecular hydrogen bonding interactions in methanol solvent for interpreting the chiroptical properties? *Spectrochimica acta. Part A, Molecular and biomolecular spectroscopy* **2020**;247:119094-119094.
49. Marta RA, Wu RH, Eldridge KR, Martens JK, McMahon TB. The sodium cation-bound dimer of theophylline: IRMPD spectroscopy of a highly symmetric electrostatically bound species. *International Journal of Mass Spectrometry* **2010**;297:76-84.
50. MacroModel version 9.8; ed. Schrödinger, LLC: New York, NY, 2010. *MacroModel version 9.8; ed. Schrödinger, LLC: New York, NY, 2010*.
51. Harder E, Damm W, Maple J, Wu C, Reboul M, Xiang JY, Wang L, Lupyan D, Dahlgren MK, Knight JL and others. OPLS3: A Force Field Providing Broad Coverage of Drug-like Small Molecules and Proteins. *Journal of Chemical Theory and Computation* **2016**;12:281-296.
52. Halgren TA. MMFF VI. MMFF94s option for energy minimization studies. *Journal of Computational Chemistry* **1999**;20:720-729.
53. Goerigk L, Grimme S. A thorough benchmark of density functional methods for general main group thermochemistry, kinetics, and noncovalent interactions. *Physical Chemistry Chemical Physics* **2011**;13:6670-6688.
54. Grimme S, Antony J, Ehrlich S, Krieg H. A consistent and accurate ab initio parametrization of density functional dispersion correction (DFT-D) for the 94 elements H-Pu. *Journal of Chemical Physics* **2010**;132:154104
55. Becke AD. Density-functional exchange-energy approximation with correct asymptotic-behavior. *Physical Review A* **1988**;38:3098-3100.
56. Halls MD, Velkovski J, Schlegel HB. Harmonic frequency scaling factors for Hartree-Fock, S-VWN, B-LYP, B3-LYP, B3-PW91 and MP2 with the Sadlej pVTZ electric property basis set. *Theoretical Chemistry Accounts* **2001**;105:413.
57. Frisch MJ, Pople JA, Binkley JS. Self-Consistent Molecular-Orbital Methods .25. Supplementary Functions for Gaussian-Basis Sets. *Journal of Chemical Physics* **1984**;80:3265-3269.
58. Tomasi J, Mennucci B, Cammi R. Quantum mechanical continuum solvation models. *Chemical Reviews* **2005**;105:2999-3093.
59. Frisch MJ, Trucks GW, Schlegel HB, Scuseria GE, Robb MA, Cheeseman JR, Scalmani G, Barone V, Mennucci B, Petersson GA and others. Gaussian 09, Revision D.01. Wallingford CT: Gaussian Inc.; 2009.
60. Bünnemann K, Pollok CH, Merten C. Explicit Solvation of Carboxylic Acids for Vibrational Circular Dichroism Studies: Limiting the Computational Efforts without Losing Accuracy. *Journal of Physical Chemistry B* **2018**;122:8056-8064.
61. Gloaguen E, de Courcy B, Piquemal JP, Pilmé J, Parisel O, Pollet R, Biswal HS, Piuzzi F, Tardivel B, Broquier M and others. Gas-Phase Folding of a Two-Residue Model Peptide Chain: On the Importance of an Interplay between Experiment and Theory. *Journal of the American Chemical Society* **2010**;132:11860–11863.

62. Bünnemann K, Merten C. Solvation of a chiral carboxylic acid: effects of hydrogen bonding on the IR and VCD spectra of [small alpha]-methoxyphenylacetic acid. *Physical Chemistry Chemical Physics* **2017**;19:18948-18956.
63. Perera AS, Cheramy J, Merten C, Thomas J, Xu YJ. IR, Raman, and Vibrational Optical Activity Spectra of Methyl Glycidate in Chloroform and Water: The Clusters-in-a-liquid Solvation Model. *Chem Phys Chem* **2018**;19:2234-2242.
64. Weirich L, Magalhaes de Oliveira J, Merten C. How many solvent molecules are required to solvate chiral 1,2-diols with hydrogen bonding solvents? A VCD spectroscopic study. *Physical Chemistry Chemical Physics* **2019**;22:1525-1533.

Graphical Abstract

